2007

Utility of thermal sharpening over Texas high plains irrigated agricultural fields

Nurit Agam
USDA-ARS, agam@agri.gov.il

William P. Kustas
USDA-ARS, Bill.Kustas@ars.usda.gov

Martha C. Anderson
USDA-ARS, martha.anderson@ars.usda.gov

Fuqin Li
USDA-ARS

Paul D. Colaizzi
USDA-ARS, Paul.Colaizzi@ARS.USDA.GOV

Utility of thermal sharpening over Texas high plains irrigated agricultural fields

Nurit Agam,[1] William P. Kustas,[1] Martha C. Anderson,[1] Fuqin Li,[1] and Paul D. Colaizzi[2]

Received 11 January 2007; revised 10 April 2007; accepted 21 June 2007; published 13 October 2007.

[1] Irrigated crop production in the Texas high plains (THP) is dependent on water extracted from the Ogallala Aquifer, an area suffering from sever water shortage. Water management in this area is therefore highly important. Thermal satellite imagery at high temporal (~daily) and high spatial (~100 m) resolutions could provide important surface boundary conditions for vegetation stress and water use monitoring, mainly through energy balance models such as DisALEXI. At present, however, no satellite platform collects such high spatiotemporal resolution data. The objective of this study is to examine the utility of an image sharpening technique (TsHARP) for retrieving land surface temperature at high spatial resolution (down to 60 m) from moderate spatial resolution (1 km) imagery, which is typically available at higher (~daily) temporal frequency. A simulated sharpening experiment was applied to Landsat 7 imagery collected over the THP in September 2002 to examine its utility over both agricultural and natural vegetation cover. The Landsat thermal image was aggregated to 960 m resolution and then sharpened to its native resolution of 60 m and to various intermediate resolutions. The algorithm did not provide any measurable improvement in estimating high-resolution temperature distributions over natural land cover. In contrast, TsHARP was shown to retrieve high-resolution temperature information with good accuracy over much of the agricultural area within the scene. However, in recently irrigated fields, TsHARP could not reproduce the temperature patterns. Therefore we conclude that TsHARP is not an adequate substitute for 100-m-scale observations afforded by the current Landsat platforms. Should the thermal imager be removed from follow-on Landsat platforms, we will lose valuable capacity to monitor water use at the field scale, particularly in many agricultural regions where the typical field size is ~100 × 100 m. In this scenario, sharpened thermal imagery from instruments like MODIS or VIIRS would be the suboptimal alternative.

Citation: Agam, N., W. P. Kustas, M. C. Anderson, F. Li, and P. D. Colaizzi (2007), Utility of thermal sharpening over Texas high plains irrigated agricultural fields, *J. Geophys. Res.*, *112*, D19110, doi:10.1029/2007JD008407.

1. Introduction

[2] Irrigated crop production in the Texas high plains (THP) is dependent on water extracted from the Ogallala Aquifer, in a basin from which withdrawals have greatly exceeded recharge since irrigation development began in the 1930–1940s. As a result, groundwater levels in the basin are severely declining, threatening the long-term economic viability of irrigated agriculture in the THP. Monitoring and management of the area's water budget is, therefore, crucial. One of the main components of regional water management is the assessment of water loss due to evaporation, which can be significant in this area because of high insolation forcing, large vapor pressure deficits, and strong regional dry-air advection [*Colaizzi et al.*, 2006]. A routine procedure for mapping daily evaporative fluxes over large areas will provide an important tool for water management in the THP.

[3] Many regional-scale evapotranspiration (ET) models use remote sensing data in the thermal wave band to estimate land surface temperature, a key indicator of surface moisture status. The regional-scale Atmosphere-Land Exchange Inverse model (ALEXI [*Anderson et al.*, 1997, 2007]) and an associated flux disaggregation technique (DisALEXI [*Norman et al.*, 2003; *Anderson et al.*, 2004b]), for example, were designed to map ET at resolutions of 10^0–10^4 m, integrating thermal remote sensing data from multiple satellite platforms. ALEXI uses coarse-resolution (5–10 km) thermal data from geostationary satellites to estimate fluxes at the continental scale, while DisALEXI runs at finer spatial resolutions suitable for agricultural management (i.e., 100–250 m) using imagery from polar-orbiting satellites or from aircraft. Routine flux evaluations with DisALEXI, suitable for local-scale water

[1] Hydrology and Remote Sensing Laboratory, Agricultural Research Service, U.S. Department of Agriculture, Beltsville, Maryland, USA.
[2] Conservation and Production Research Laboratory, Agricultural Research Service, U.S. Department of Agriculture, Bushland, Texas, USA.

0148-0227/07/2007JD008407

management applications, will require thermal imagery at both high spatial and high temporal resolution.

[4] To date, routine, sub-field-scale spatial resolution (~100 m or finer) thermal maps, fully covering the U.S., are acquired only with the Thematic Mapper (TM) on Landsat 5, which has a revisit cycle of 16 days, yielding at best monthly or bimonthly coverage when cloud cover is considered. The Enhanced Thematic Mapper Plus (ETM+) instrument on Landsat 7 is currently suffering data loss due to failure of the scan-line corrector (SLC; http://landsat.usgs.gov/data_products/slc_off_data_products/slc_off_background.php), while image acquisitions with the Advanced Spaceborne Thermal Emission and Reflection Radiometer (ASTER) must be scheduled and therefore coverage is sporadic [e.g., *Abrams*, 2000]. Continuation of thermal band imaging on Landsat Data Continuity Mission (LDCM; http://www.ldcm.nasa.gov) platform is uncertain, and such high-resolution thermal data may soon be unavailable at any temporal resolution. The Moderate Resolution Imaging Spectroradiometer (MODIS; http://modis.gsfc.nasa.gov) system and the Advanced Very High Resolution Radiometer (AVHRR; http://noaasis.noaa.gov/NOAASIS/ml/avhrr.html) provide daily thermal band imagery but at 1 km spatial resolution, which is too coarse for agricultural management.

[5] To address the current and impending gaps in high-resolution thermal data availability, *Kustas et al.* [2003] developed a technique for spatially sharpening moderate resolution thermal images using information regarding vegetation cover amount derived from shortwave imagery, typically collected at higher spatial resolution, 4–16 times finer than the thermal band resolution. The principal idea behind the sharpening procedure (TsHARP) exploits the negative relationship between the surface temperature and fraction of vegetation cover (detailed description is provided in section 2.1). If successful over the landscapes characteristic of the THP, this sharpening procedure could be applied to MODIS thermal imagery to provide near daily field-scale evaluations of ET, which could be a valuable tool in conserving water in the Ogallala Aquifer.

[6] The objective of this study was to examine the utility of this image sharpening technique (TsHARP) in retrieving land surface temperature at high spatial resolution over agricultural regions of the THP.

2. Methodology

2.1. Sharpening Procedure

[7] The TsHARP algorithm was developed by *Kustas et al.* [2003] and utilized by *Anderson et al.* [2004b] to retrieve high-resolution ET maps over experimental sites in the Southern Great Plains (SGP). TsHARP was recently refined in an application over the upper Midwest corn and soybean production region in central Iowa during the growing season of 2002 [*Agam et al.*, 2007]. The basic algorithm exploits the natural covariation that typically exists between surface temperature and vegetation cover amount. Where evaporative fluxes are not energy limited, areas with higher vegetation cover tend to have lower surface temperature because of cooling by transpiration. Bare, dry soil is generally hotter than is healthy transpiring vegetation. It is assumed that this covariation exists within a sensor scene at multiple spatial resolutions.

[8] The revised sharpening procedure developed by *Agam et al.* [2007] uses a simplified form of fractional vegetation cover ($f_C s$, equation (1)) derived from the fractional cover-NDVI relationship given by *Choudhury et al.* [1994], setting the NDVI scaling coefficients $NDVI_{max}$ and $NDVI_{min}$ to 1 and 0, respectively (see *Agam et al.* [2007] for details of the development of $f_C s$):

$$f_C s = 1 - (1 - NDVI)^{0.625} \tag{1}$$

A least squares regression is performed between T_R and $f_C s$, after NDVI has been aggregated to the coarser thermal resolution ($NDVI_{low}$):

$$\hat{T}_R(NDVI_{low}) = a_0 + a_1 f_C s_{low} = a_0' - a_1'(1 - NDVI_{low})^{0.625} \tag{2}$$

Here the "hat" symbol indicates a temperature value predicted using the vegetation index (VI) regression equation. This regression relationship is then applied to the NDVI data at their finer, native resolution ($NDVI_{high}$):

$$\hat{T}_R\left(NDVI_{high}\right) = a_0' - a_1'\left(1 - NDVI_{high}\right)^{0.625} \tag{3}$$

Errors in the least squares regression, due to forces driving surface temperatures other than vegetation cover amount (e.g., soil moisture), can be assessed at the coarse scale:

$$\Delta\hat{T}_{R\ low} = T_{R\ low} - \hat{T}_R(NDVI_{low}) \tag{4}$$

The coarse-scale residual field is added back into the sharpened map such that the original temperature field is recovered through reaggregation. The sharpened subpixel temperatures within each coarse pixel are therefore computed via:

$$\hat{T}_{R\ high} = \hat{T}_R\left(NDVI_{high}\right) + \Delta\hat{T}_{R\ low} \tag{5}$$

where the first term of the right-hand side is evaluated using equation (3), and the second residual term from equation (4) is constant over the coarse pixel area.

[9] This procedure requires that a range of surface temperature and vegetation cover fraction be present within the image scene, in order to develop a significant regression relationship. TsHARP therefore does not perform well over scenes in which there is little variability in surface temperature; for example during nighttime or early morning, or in areas where surface conditions are relatively homogeneous. However, the practical benefits of sharpening such scenes are limited. Homogeneous scenes will not profit from sharpening, and most remote-sensing-based energy balance models are applied midmorning and midafternoon, times when TsHARP would be most useful and applicable.

2.2. Study Area and Satellite Imagery

[10] The study area was composed of a Landsat ETM+ scene (row 36, path 31) from 2002, overlying the northern part of the Texas–New Mexico state borderline (centered at 34°37′N, 102°53′W). This area is part of the southern high

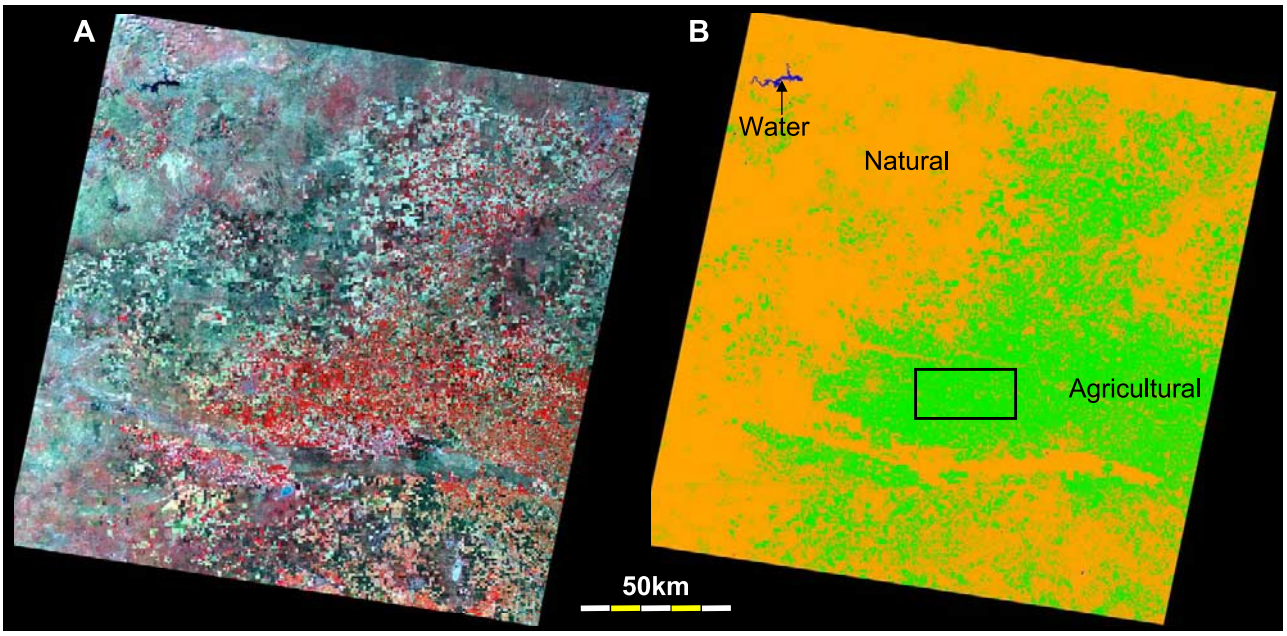

Figure 1. Study area: (a) false-color image of a Landsat ETM+ scene (row 36, path 31) overlying the northern part of the Texas–New Mexico state borderline (centered at 34°37′N, 102°53′W) acquired on 22 September 2002 and (b) a land cover classification: dark blue, water; orange, natural land cover; green, agricultural land cover.

plains, within the larger Great Plains of the western United States. The scene was classified into general land cover categories of agricultural land, natural vegetation, and open water using an unsupervised classification technique applied to 5 scenes acquired on 15 April, 2 June, 20 July, 22 September and 9 November 2002. The span in dates captured phenological signatures, allowing good discrimination between agricultural and natural land cover classes. Figure 1a is a false color image of the study area, composed of various land cover classes including agricultural fields (both irrigated and rainfed; red tones), natural vegetation (blue grey tones), and water (dark blue) (see classification in Figure 1b).

[11] The sharpening algorithm was tested over the 22 September scene. Of the scenes available during 2002, this scene provided the most variability in vegetation cover and moisture conditions (due to irrigation) over the THP irrigated agricultural area. September is a relatively dry month in comparison with June–August. During this month, the cotton crops are reaching maturity and are thus unlikely to be irrigated, while emerging winter wheat crops are typically receiving irrigation.

[12] Spaceborne multispectral imagery from the Landsat 7 ETM+, acquired on 22 September 2002 (prior to failure of the SLC), provided visible/near-infrared (VIS/NIR) and thermal infrared (TIR) data at 30 and 60 m native resolution, respectively. The process for retrieving surface radiometric temperature, T_R, from the single thermal band on Landsat 7 is fully detailed by *Li et al.* [2004]. In short, the at-sensor brightness temperatures were atmospherically corrected using MODTRAN [*Berk et al.*, 1998], and then corrected for emissivity effects using a fractional cover mixture model [*Sobrino et al.*, 2001].

2.3. Simulated Sharpening Experiment

[13] To test the ability of TsHARP to retrieve high-resolution structure in surface temperature fields, the thermal Landsat image was aggregated to coarser resolution, and then sharpened and compared to the original image data. While the ultimate goal of this research is to apply TsHARP to MODIS thermal data, it is important to first optimize and verify the base performance of the algorithm in a best case scenario, independent of errors introduced by intersensor comparisons. MODIS-Landsat thermal image comparisons are complicated by differences in view angle, pixel registration, and overpass time. While such comparisons are being conducted and are essential to the overall assessment of the sharpening algorithm, they will be presented in a forthcoming paper.

[14] The Landsat ETM+ T_R and NDVI images were aggregated to a resolution of 960 m, simulating the native resolutions of MODIS/AVHRR thermal bands. Since NDVI has been demonstrated to aggregate linearly [*Hall et al.*, 1992; *Friedl et al.*, 1995; *De Cola*, 1997; *Anderson et al.*, 2004a], NDVI data were aggregated by simple areal average, while the T_R data were first converted to radiance values and then the radiances were aggregated. Conversion to radiance was carried out following the Stephan-Boltzmann law, $R = \varepsilon\sigma T_R^4$, in which R is the thermal radiance, σ is Stephan-Boltzmann constant, and ε is the surface emissivity. Previous studies show the applicability of the forth power of Stephan-Boltzmann law to narrow thermal bands [e.g., *Becker and Li*, 1990; *Norman and Becker*, 1995]. In addition, the T_R and NDVI images were also aggregated to 240, 120, and 60 m, simulating a range in potential target (sharpened) resolutions. The T_R images at the finer resolutions were used as reference images ($T_{R\ ref}$) for validating temperature retrieval accuracy.

Table 1. Regression Parameters Derived From the T_R-f_Cs Relationship at 60, 120, 240 and 960 m Resolution for the Entire Scene, the Nonagricultural Area, and the Agricultural Area[a]

	N	AVG f_Cs (Fraction)	AVG T_R, °C	STD f_Cs (Fraction)	STD T_R, °C	STD T_R Subpixel, °C	a_0	a_1	r^2
				All					
60 m	9,104,732	0.25	29.11	0.10	2.77	1.34	−11.65	31.97	0.19
120 m	2,276,646	0.25	29.11	0.10	2.70	1.21	−11.95	32.04	0.20
240 m	569,300	0.24	29.11	0.09	2.61	1.06	−12.08	32.07	0.18
960 m	35,413	0.24	29.12	0.07	2.30	NA	−11.07	31.81	0.11
				Natural (∼63%)					
60 m	5,731,021	0.22	29.55	0.07	2.53	1.28	−3.55	30.32	0.01
120 m	1,498,446	0.22	29.53	0.06	2.47	1.17	−5.42	30.72	0.02
240 m	380,638	0.22	29.50	0.06	2.43	1.05	−5.30	30.67	0.02
960 m	23,600	0.23	29.35	0.06	2.31	NA	−7.15	30.96	0.01
				Agricultural (∼37%)					
60 m	3,372,924	0.29	28.35	0.14	3.00	2.27	−13.05	32.20	0.37
120 m	776,090	0.29	28.31	0.14	2.94	2.16	−13.48	32.28	0.39
240 m	187,721	0.29	28.32	0.13	2.81	1.95	−13.84	32.36	0.39
960 m	11,753	0.28	28.66	0.08	2.21	NA	−14.43	32.67	0.28

[a]Also shown are average and standard deviation in f_Cs and T_R, and the average subpixel standard deviation in T_R at the 960-m scale. N, number of pixels; AVG, average; STD, standard deviation; a_o and a_1, parameters of the regression line $Y = a_0 + a_1X$, in which $Y - T_R$ and $X - f_C$s; r^2, coefficient of determination; NA, not applicable.

[15] The sharpening algorithm was then applied to the coarse-resolution (960 m) T_R data, using the multiscale NDVI information to generate temperature maps with target resolutions of 240, 120 and 60 m. The 240 m resolution simulates the sharpening of MODIS thermal band to the resolution of the MODIS VIS/NIR bands, while the 120 and 60 m analyses demonstrate the additional value in terms of information content of the Landsat thermal band resolutions (TM and ETM+, respectively).

2.4. Statistical Evaluation

[16] The level of agreement between the reference ($T_{R\,ref}$) and sharpened ($\hat{T}_{R\,high}$; equation (5)) temperature fields was assessed by means of mean-absolute-error (*MAE*). This measure, in comparison with the widely used root-mean-square error (*RMSE*), has the advantage of being less sensitive to the distribution of the errors and number of data points [*Willmott and Matsuura*, 2005]. Note that in this study, $RMSE \approx 1.14\ MAE$ ($r^2 = 0.99$). In addition, a baseline case, representing no sharpening, i.e., no incorporation of high-resolution information (uniT_R) was also computed by assigning each subpixel the temperature of the corresponding coarse pixel. *MAE* was then computed between uniT_R and $T_{R\,ref}$ as well. For each target resolution then, two values of *MAE* were computed: comparing $T_{R\,ref}$ with $\hat{T}_{R\,high}$ (sharpened temperature field) and with uniT_R (unsharpened field). The difference in *MAE* between the two methods can be used to determine the effectiveness of the sharpening technique.

3. Results and Discussion

3.1. Scene Characteristics

[17] The sharpening algorithm requires that there be good correlation between surface temperature and vegetation index, and thus it is instructive to examine this relationship within the context of the full Landsat scene to understand possible limitations and error sources in applications to this kind of landscape. In contrast to the uniform rainfed agricultural region in central Iowa, where one T_R-f_Cs relationship was found sufficient to sharpen the entire Landsat scene [*Agam et al.*, 2007], significant variability in land use can be found in the THP, particularly the contrast between the natural and agricultural areas. Using measurements collected over tallgrass prairie in northeastern Kansas, *Friedl and Davis* [1994] demonstrated that correlations between T_R and NDVI improved when the data were stratified by land cover type. Therefore two different approaches were examined: (1) sharpening the entire scene using one general regression, the rationale being that if good results are obtained the sharpening algorithm will be simpler, and (2) classifying the scene into agricultural and natural areas and sharpening each land use separately.

[18] The T_R-f_Cs relationship, determined by the regression parameters and coefficient of determination, was examined for the entire scene, as well as for the natural and agricultural areas separately, at the four studied resolutions (60, 120, 240, and 960 m); along with the mean and standard deviation in T_R and f_Cs at each resolution (Table 1). The average temperature of the natural area was ∼1°C higher than that of the agricultural area, reflecting its lower fraction vegetation cover. While the averages remain constant with resolution, the standard deviations decrease toward coarser resolutions, because of the narrowing of the dynamic range with aggregation. This decrease in variability in f_Cs and T_R with coarsening resolution is most notable in the more heterogeneous agricultural area.

[19] The vegetation in the nonagricultural parts of the scene is sparse, consisting primarily of native grass and small shrubs spaced ∼1–10 m, but relatively uniformly distributed at the kilometer scale. In comparison, variability in cultivation practices, crop type, irrigation strategy and planting date within the agricultural land class results in a distribution spanning the full range in f_Cs present in the scene (up to 0.6). In addition, there is less subpixel heterogeneity in temperature at the kilometer scale for the natural vegetation class. Table 1 lists the average standard deviation in reference temperatures ($T_{R\,ref}$) at 60, 120 and 240 m, computed by class for each 960 m pixel and

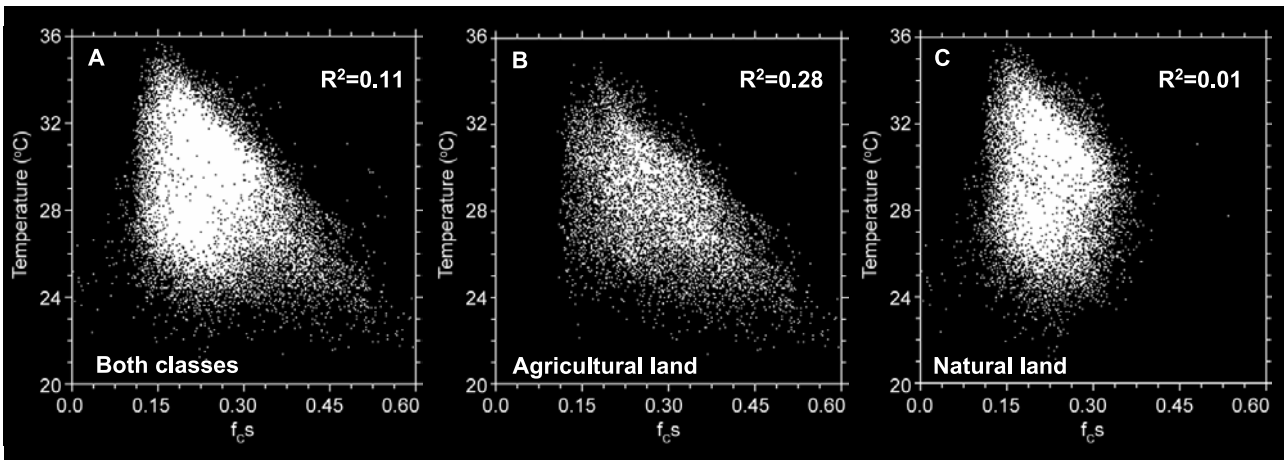

Figure 2. Scatterplots at 960 m resolution of temperature versus the simplified form of fractional vegetation cover (f_Cs) for the (a) entire scene, (b) agricultural land cover, and (c) natural land cover classes.

averaged over the whole scene, demonstrating that coarse-scale pixels containing natural land cover tend to be more homogeneous. At resolutions finer than 1 km, field boundaries in agricultural areas are still resolvable, since the typical field size is on the order of 800 m. On the other hand, a significant increase in subpixel variability occurs at 1 km resolution, since multiple field boundaries are likely to be encompassed in each pixel.

[20] The regression parameters were fairly insensitive to resolution (Table 1), supporting the assumption that the T_R-f_Cs covariation exists within this sensor scene at multiple spatial resolutions. An example of the scatterplot of T_R versus f_Cs is given for the 960 m resolution (Figure 2a, excluding pixels classified as water) showing a large scatter in T_R at low f_Cs, resulting in a weak coefficient of determination between these two variables (r^2 = 0.11). The r^2 values between T_R and f_Cs for the natural and the agricultural areas were 0.01 and 0.28 (Figures 2b and 2c), respectively. In comparison, *Agam et al.* [2007] found r^2 of 0.4–0.7 over a purely rainfed agriculture scene in central Iowa. The lower correlations in this Texas scene likely result from surface moisture variability due to localized irrigation systems. High-resolution variability in surface temperature due to patchy moisture conditions cannot be retrieved through the VI-based thermal sharpening technique described here, although moisture and other non-VI related effects are included at the coarse (native) scale because of reintroduction of the sharpening residuals, ΔT_R. These scene characteristics suggest that sharpening may be less effective for the natural land cover class.

3.2. Sharpening Stratification by Land Cover Class

[21] The higher correlation between f_Cs and T_R for the agricultural class demonstrated in Table 1 and Figure 2 suggests that there may be benefit in isolating these pixels prior to sharpening. TsHARP was therefore executed twice: using regression parameters derived (1) over the entire scene and (2) over pixels classified as agricultural area only. Error statistics at the three target resolutions are listed in Table 2. Temperature fields retrieved through TsHARP showed a significant improvement in comparison with uniT_R for the agricultural class, reducing errors by 32–36%, as described in greater details in section 3.3. A smaller improvement is observed for the scene as a whole (14–18% reduction in MAE). The low correlation between T_R and f_Cs for the natural land cover class does not allow development of meaningful regression parameters for that class in isolation. This is because the surface temperature in the naturally vegetated areas has smaller spatial variability, with a length scale of heterogeneity that is significantly less than the original spatial resolution of the thermal data (60 m).

[22] Despite the improvement achieved by sharpening the agricultural areas in comparison with uniT_R, the errors are larger for the agricultural class than for the scene as a whole. This is because the natural area (~65% of the pixels) is relatively homogeneous, thus its structure is less dependent on resolution over the studied range of scales. When these areas are included in the statistics, they reduce the overall error, "masking" the real error magnitude of the scale-sensitive agricultural areas.

[23] In summary, in this landscape it appears that sharpening does not improve error statistics over parts of the scene composed of natural land cover because these areas are relatively homogeneous even at the 60-m scale. In

Table 2. Mean Absolute Errors (MAE) Obtained Comparing the Sharpened Temperatures (TsHARP) at 60, 120 and 240 m Resolution and the Original Coarse-Resolution (960 m) Temperatures (uniT_R) to the Respective Reference Temperature Fields (1) Including the Entire Scene and (2) Including the Agricultural Area Only

	Mean Absolute Errors, °C			
	Entire Scene		Agricultural Area Only	
Target Spatial Resolution, m	TsHARP	uniTR	TsHARP	uniTR
60	0.91	1.06	1.06	1.55
120	0.82	0.97	0.94	1.43
240	0.68	0.83	0.80	1.25

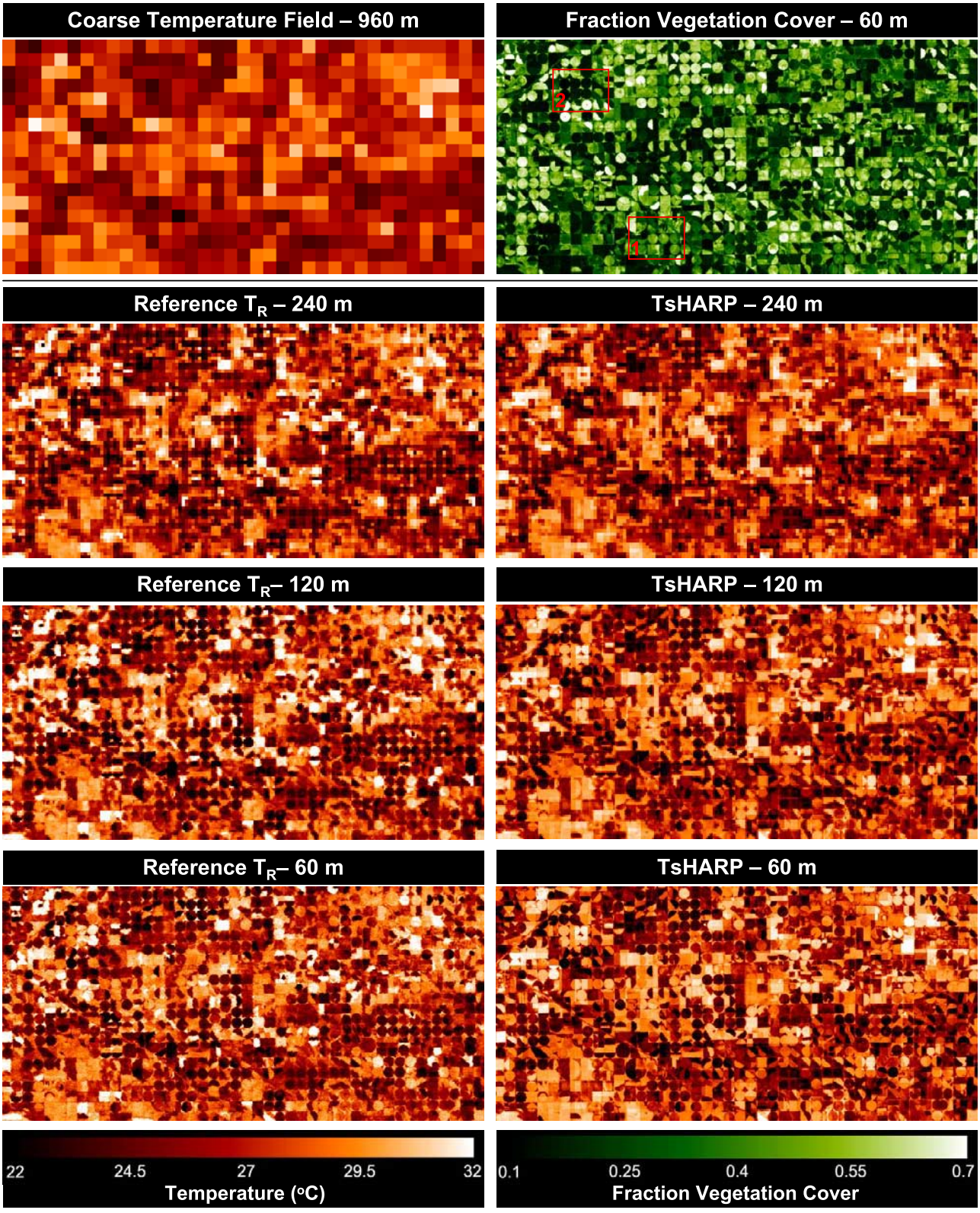

Figure 3. Temperature fields (in red hues) and simplified fraction vegetation (f_Cs) field (green hues) of the subset area demarcated in Figure 1b. (left) Reference temperature fields at 960, 240, 120, and 60 m spatial resolutions. (right) Corresponding sharpened fields for the 240, 120, and 60 m resolutions.

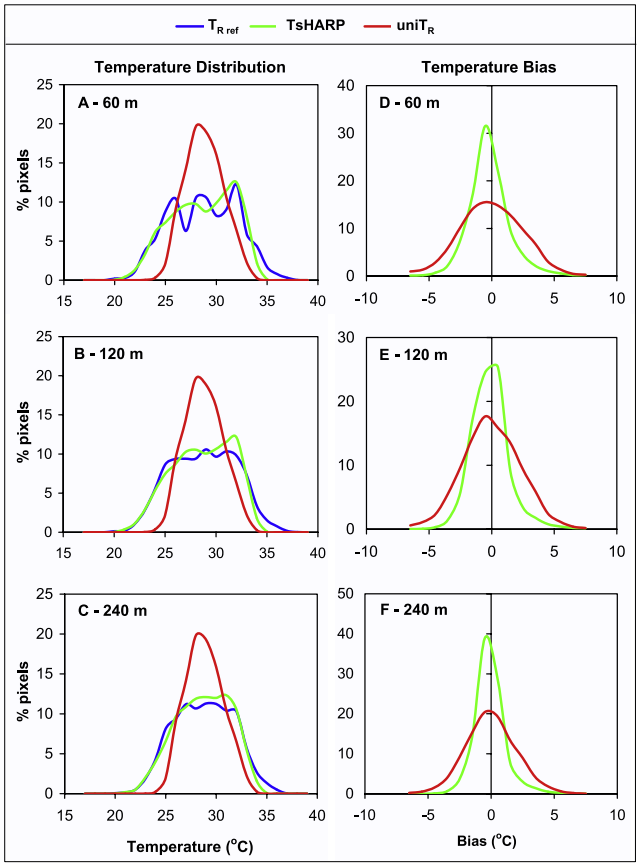

Figure 4. Distribution of the reference ($T_{R\ ref}$), the sharpened (TsHARP), and the uniformly distributed ($uniT_R$) temperatures at (a) 60, (b) 120, and (c) 240 m resolutions. Error distributions, resulting from subtracting the reference temperature fields from TsHARP and $uniT_R$, for the (d) 60, (e) 120, and (f) 240 m resolutions.

contrast, significant high-resolution temperature information can be retrieved from the vegetation cover relationship over agricultural areas, as demonstrated below.

3.3. Sharpening Over Agricultural Areas

3.3.1. Descriptive Analysis

[24] To demonstrate the resolution dependence of information content and sharpening accuracy in temperature fields over the agricultural parts of this Landsat scene, we focus on the small subimage (~36 by 17 km) demarcated in Figure 1b. Figure 3 shows the spatial distribution of temperature and f_cs over this subarea at 960 and 60 m resolution, respectively. Also shown are the reference and sharpened temperature fields at 240, 120 and 60 m spatial resolutions.

[25] Individual fields (with typical size of ~800 × 800 m) cannot be distinguished in the 960-m resolution temperature map. The fields are marginally resolved at 240 m, but given the significant variation in cover and moisture conditions between adjacent fields, a large proportion of the pixels represent mixed surface conditions. The 120 m resolution images clearly resolve individual fields, providing a reasonable spatial resolution for agricultural applications in this area. At 60 m, within-field variations can be detected, providing useful information for precision agricultural management in the Texas high plains. To monitor evapotranspiration at the field scale over agricultural areas with similar spatial characteristics, a minimum thermal band spatial resolution of ~100 m will be required. At this scale, the sharpening algorithm retrieves the spatial structures observed in the reference images with good fidelity. While the reconstruction errors increase at finer target resolutions (Table 2), they remain within a reasonable range (~1°C).

3.3.2. Statistical Analysis

[26] The temperature distributions of the reference ($T_{R\ ref}$), the sharpened (TsHARP) and the nonsharpened ($uniT_R$) fields at the three resolutions investigated are plotted in Figures 4a–4c. The dynamic range of the reference fields, excluding the 5% tails of the distributions (hereafter referred to as the 90% dynamic range), is 8.9, 8.4, and 7.7°C, for the 60, 120, and 240 m, respectively, i.e., widest at the 60 m resolution and narrowest at 240 m. The $uniT_R$ image at 960 m resolution has a narrower dynamic range of 5.1°C (excluding the 5% tails). TsHARP distributions follow the reference fields much closer than does $uniT_R$, with 90% dynamic range of 8.3, 7.9, and 5.1°C, for the 60, 120, and 240 m, respectively. Figures 4d–4f show the distribution of the errors computed by subtracting TsHARP and $uniT_R$ images from the reference temperature fields. The significantly higher peak of TsHARP around zero, compared to the lower and wider distribution of $uniT_R$ errors, further demonstrates the utility of the sharpening algorithm.

[27] This improvement in image fidelity can also be seen in scatterplots comparing the TsHARP and $uniT_R$ fields with the reference temperature fields (Figure 5). The slopes of the regressions of TsHARP versus $T_{R\ ref}$ are much closer to 1 than those of $uniT_R$ (0.81–0.84 versus 0.38–0.46, respectively). The coefficients of determination are also significantly higher for the sharpened compared to nonsharpened fields (~0.8 versus ~0.5). It is therefore concluded that the sharpening algorithm significantly improved, both visually and statistically, the temperature fields over the irrigated agricultural area.

3.4. Error Sources in TsHARP Algorithm

[28] While the potential of TsHARP to provide sharpened temperature images has been demonstrated in the previous section, it cannot completely reconstruct the subpixel temperature structure in the reference fields. Two main sources of errors have been identified: (1) TsHARP only accounts for soil moisture at the coarse scale and cannot detect subpixel variations in soil moisture (due to irrigation in this example) and (2) the temperature residual field computed from equation (4) form boxy discontinuities in some parts of the sharpened temperature field. In order to demonstrate these errors, two small subareas (demarcated in Figure 3) were selected. In the first area (enlarged in Figures 6a–6d), temperature is strongly correlated with the vegetation cover, and TsHARP accurately reproduces the high-resolution temperature field, even detecting some within-field variations in temperature.

[29] In contrast, the second subarea exemplifies the shortcomings of TsHARP, as illustrated by Figures 6e–6i. The yellow circles mark a center pivot irrigation field, divided diagonally into two halves. The fraction vegetation cover of the southwestern (SW) half is low, indicating nearly bare

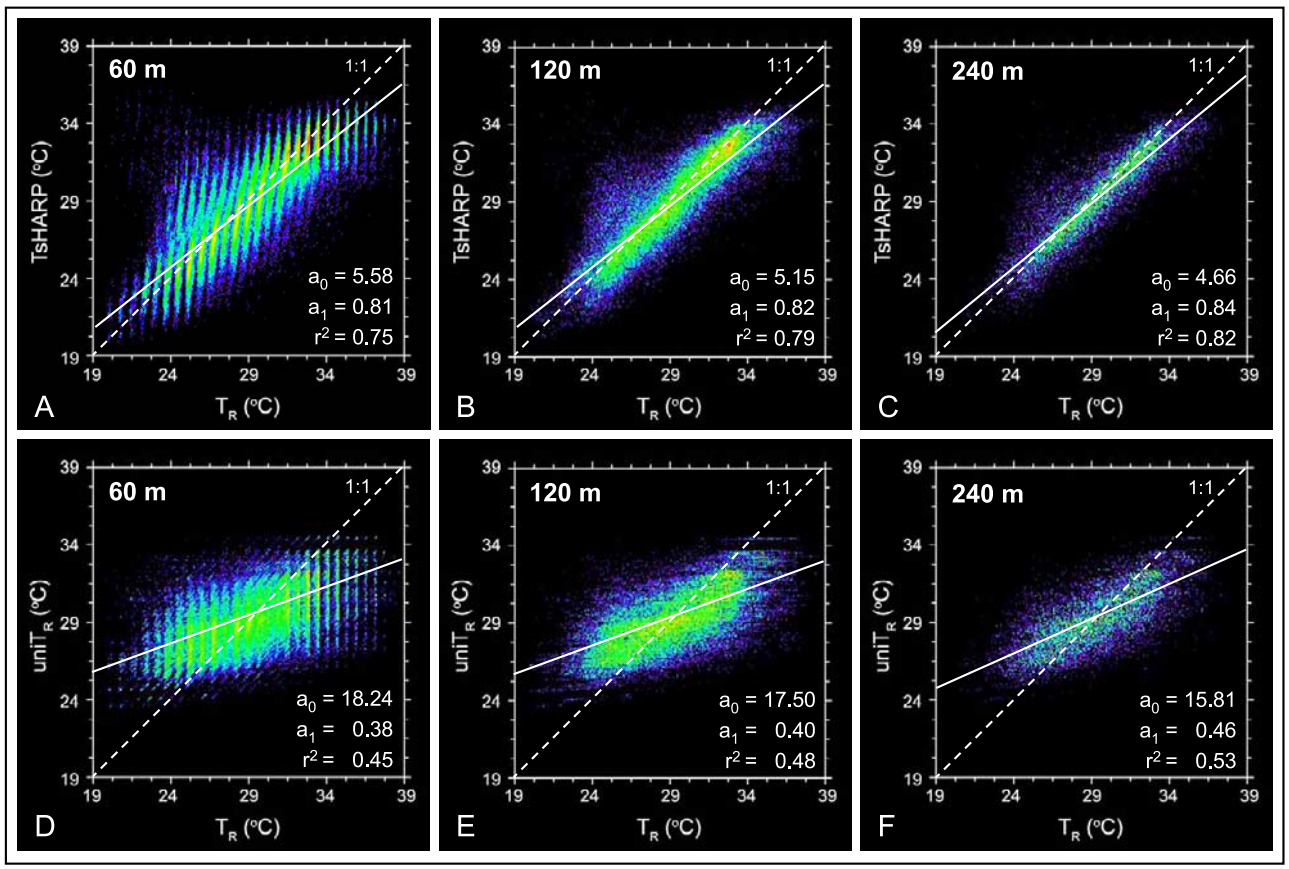

Figure 5. Scatterplots of (a–c) TsHARP and (d–f) UniT_R fields versus the reference temperature fields at 60 m, 120 m and 240 m resolution. The variables a_0 and a_1 are the regression coefficients for the line $Y = a_0 + a_1X$, and the dashed line represents perfect agreement.

soil conditions, while the northeast (NE) half has a higher fraction cover (Figure 6e). The reference temperature field (Figure 6f), however, shows the lower cover half of the field has lower surface temperature, likely indicating more recent irrigation. This behavior is contrary to the scene-scale T_R-f_Cs relationship defining the sharpening equation, and thus the retrieved temperature patterns in this field are reversed. The adjacent field to the south (not marked) had a similar distribution of cover fraction, but uniform surface temperature, suggesting the whole field was recently irrigated. The TsHARP approach was unable to detect subpixel variations in soil moisture (due to irrigation in this example), which may result in erroneous temperature retrievals.

[30] The second error source, related to the temperature residual field computed from equation (4), is exemplified by the 4 pivot-irrigated fields within the dark blue rectangles. The artificial discontinuities (box-like in appearance) displayed in the sharpened temperature field (Figure 6h) is imposed by a strong, positive residual to the T_R-f_cs relation at the native 960 m resolution, which is significantly larger than neighboring residuals (Figure 6i). The four low vegetation cover fields overlapping this residual are significantly warmer than would be expected from the scene-level regression equation: the soil here is likely exceptionally dry. However, the residual is not distributed appropriately across the fields, but rather concentrated in the single coarse pixel most fully contained within the field boundaries. This problem is exacerbated in this case because the expected patterns in moisture variability (at the field or multifield scale) are close to, but not well resolved at the native thermal band resolution.

[31] The contrast between these two subareas is further demonstrated by their error maps (Figures 6j and 6k). Note that positive errors mean retrieved temperatures were higher than the reference temperatures and are represented by the warmer hues of the image. The error map for the first subarea is significantly more uniform than that of the second subarea, reflecting the better ability of the sharpening algorithm to reproduce the surface temperatures of this subarea. The error map of the second has clear spatial patterns, matching the limitations of TsHARP discussed above. In general, fields with large negative errors were probably wet from recent irrigation, while fields with large positive errors may indicate water stress conditions.

[32] In summary, while TsSHARP is able to reconstruct structure in surface temperature fields related to vegetation cover amount, it is unable to retrieve that component driven by subpixel variability in moisture conditions. Image sharpening is therefore not a replacement for a high-resolution thermal imaging sensor, particularly for purposes of field-scale monitoring of evapotranspiration and moisture stress in irrigated areas. Nevertheless, in the absence of high-resolution thermal imagery, TsHARP seems to be able to enhance the resolution of simulated MODIS images over

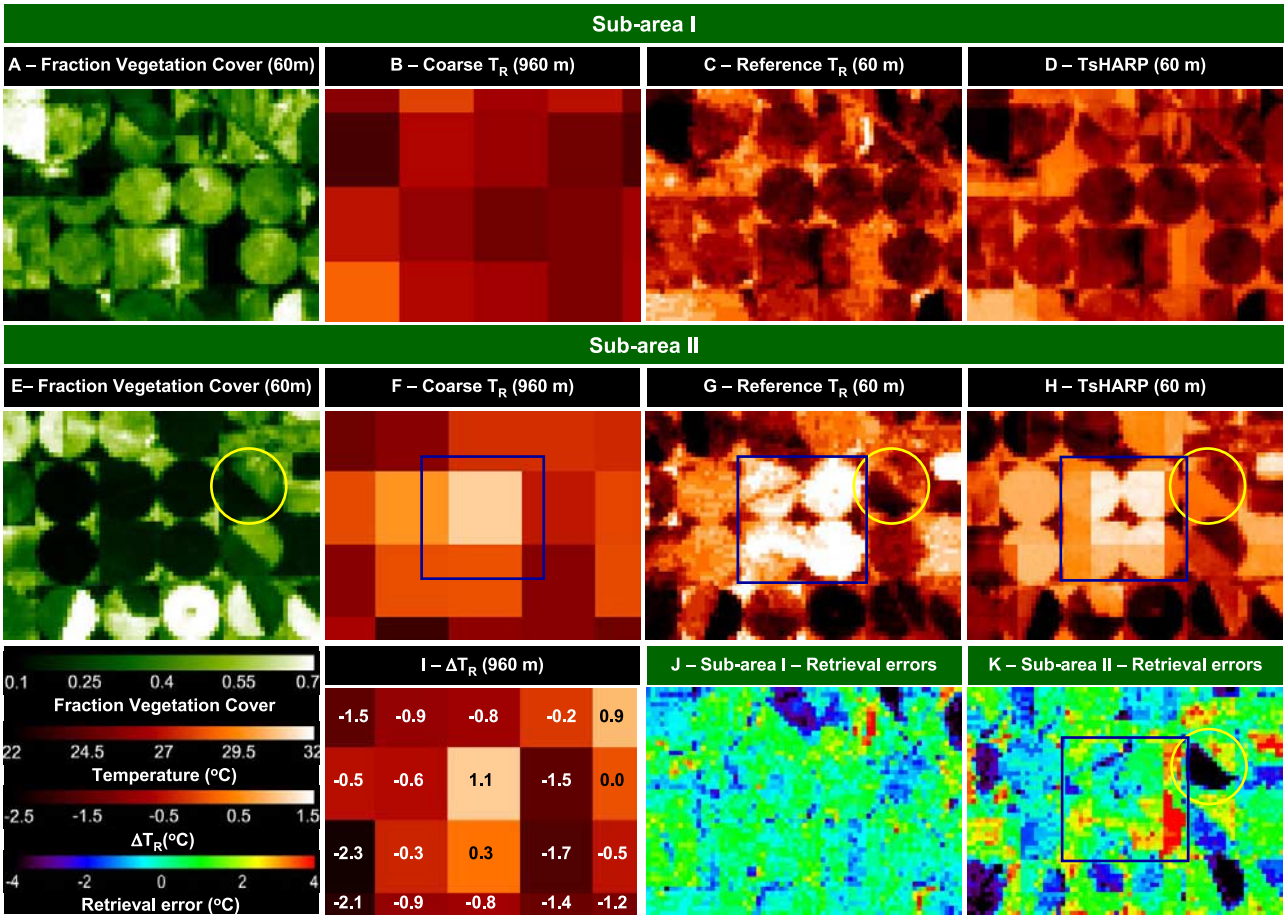

Figure 6. Subareas demonstrating (a–d) successful applications of TsHARP (subarea I) and (e–h) problematic applications (highlighted in yellow circle and dark blue rectangle in subarea II). (i) Residuals (equation (4)) for subarea II. Error maps of subareas (j) I and (k) II.

the agricultural fields of the Texas high plains, and provide in many instances fairly reliable field and subfield surface temperature distributions.

4. Conclusions

[33] A thermal image sharpening algorithm (TsHARP) was tested over the Texas high plains using a Landsat ETM+ scene acquired on 22 September 2002, examining the improvement of high-resolution temperature retrieval accuracy when incorporating land use classification information. The algorithm uses scene-dependent correlations derived between surface temperature (T_R) and vegetation indices serving as a proxy for cover amount (f_Cs) to increase the resolution of thermal band imagery to that of associated shortwave reflectance bands. Coarse-scale temperature images at 960 m resolution, generated through aggregation of the native 60 m resolution thermal data, were sharpened to 240, 120 and 60 m and compared with reference images aggregated directly to the target resolutions.

[34] Pixels in the natural vegetation class were distributed over a compressed range of fraction vegetation cover, resulting in low correlation (r^2 = 0.01) between T_R and f_Cs. Meaningful regression parameters for this area in isolation could therefore not be derived. Furthermore, the small length scale of heterogeneity within these natural areas (~1–10 m) is significantly less than the original spatial resolution of the thermal data (60 m). Therefore the sharpening algorithm did not retrieve additional useful subpixel information over areas of the Landsat scene composed of natural vegetation.

[35] In contrast, significant high-resolution temperature information could be successfully retrieved from the vegetation cover relationship over the agricultural areas within the scene, characterized by fields with typical size of ~800 × 800 m. An optimal target resolution for agricultural applications in this area was found to be ≤100 m, such that individual fields are well resolved. At this scale, the sharpening algorithm retrieved the spatial structures observed in the reference images with good fidelity and the reconstruction errors remained within a reasonable range (~1°C).

[36] Two error sources in TsHARP were identified and discussed. The first is caused by variability in moisture conditions occurring at scales smaller than the native thermal band resolution, e.g., due to recent irrigation. The current form of the algorithm only reconstructs subpixel temperature variability that is correlated with vegetation cover amount.

[37] The second error source relates to the temperature residual field itself. If the residual associated with a given pixel is exceptionally different from those of its neighboring pixels, a boxy artifact at the scale of the native pixel resolution will be apparent in the sharpened temperature field. This effect is most evident when the coarse pixel scale exceeds the dominant length scale of heterogeneity within the landscape, and when strong isolated residuals due, e.g., to patchy moisture conditions are present.

[38] The sharpening algorithm does appear to have potential for generating useful high-temporal sub-field-scale temperature information from MODIS thermal images. However, this study was carried out using aggregated Landsat imagery rather than real MODIS data; therefore it is likely to expect larger errors when applying the procedure to MODIS data. The results of this study suggest that TsHARP is not an adequate substitute for the 100-m scale observations afforded by the current Landsat platforms in areas with significant moisture variations. Should the thermal imager be removed from the LDCM, we will lose valuable capacity to monitor water use over heterogeneous landscapes at the field scale.

[39] **Acknowledgments.** This research was supported by Vaadia-BARD Postdoctoral Fellowship Award FI-371-2005 from BARD, the United States–Israel Binational Agricultural Research and Development Fund.

References

Abrams, M. (2000), The Advanced Spaceborne Thermal Emission and Reflection Radiometer (ASTER): Data products for the high spatial resolution imager on NASA's Terra platform, *Int. J. Remote Sens.*, *21*, 847–859.

Agam, N., W. P. Kustas, M. C. Anderson, F. Li, and C. M. U. Neale (2007), A vegetation index based technique for spatial sharpening of thermal imagery, *Remote Sens. Environ.*, *107*, 545–558.

Anderson, M. C., J. M. Norman, G. R. Diak, W. P. Kustas, and J. R. Mecikalski (1997), A two-source time-integrated model for estimating surface fluxes using thermal infrared remote sensing, *Remote Sens. Environ.*, *60*, 195–216.

Anderson, M. C., C. M. U. Neale, F. Li, J. M. Norman, W. P. Kustas, H. Jayanthi, and J. Chavez (2004a), Upscaling ground observations of vegetation water content, canopy height, and leaf area index during SMEX02 using aircraft and Landsat imagery, *Remote Sens. Environ.*, *92*, 447–464.

Anderson, M. C., J. M. Norman, J. R. Mecikalski, R. D. Torn, W. P. Kustas, and J. B. Basara (2004b), A multi-scale remote sensing model for disaggregating regional fluxes to micrometeorological scales, *J. Hydrometeorol.*, *5*, 343–363.

Anderson, M. C., J. M. Norman, J. R. Mecikalski, J. A. Otkin, and W. P. Kustas (2007), A climatological study of evapotranspiration and moisture stress across the continental United States based on thermal remote sensing: 1. Model formulation, *J. Geophys. Res.*, *112*, D10117, doi:10.1029/2006JD007506.

Becker, F., and Z.-L. Li (1990), Temperature-independent spectral indices in thermal infrared bands, *Remote Sens. Environ.*, *32*, 17–33.

Berk, A., L. S. Bernstein, G. P. Anderson, P. K. Acharya, D. C. Robertson, J. H. Chetwynd, and S. M. Adler-Golden (1998), MODTRAN cloud and multiple scattering upgrades with application to AVIRIS, *Remote Sens. Environ.*, *65*, 367–375.

Choudhury, B. J., N. U. Ahmed, S. B. Idso, R. J. Reginato, and C. S. T. Daughtry (1994), Relations between evaporation coefficients and vegetation indices studied by model simulations, *Remote Sens. Environ.*, *50*, 1–17.

Colaizzi, P. D., P. H. Gowda, T. H. Marek, and D. O. Porter (2006), Reducing Ogallala withdrawals by changing cropping and irrigation practices in the Texas High Plains, paper presented at Ground Water and Surface Water Under Stress: Competition, Interaction, Solutions, Boise, Id., U. S. Comm. on Irrigation and Drainage, Denver, Colo.

De Cola, L. (1997), Multiresolution covariation among Landsat and AVHRR vegetation indices, in *Scale in Remote Sensing and GIS*, edited by D. A. Quattrochi and M. F. Goodchild, pp. 73–91, CRC Press, Boca Raton, Fla.

Friedl, M. A., and F. W. Davis (1994), Sources of validation in radiometric surface temperature over a tallgrass prairie, *Remote Sens. Environ.*, *48*, 1–17.

Friedl, M. A., F. W. Davis, J. Michaelsen, and M. A. Moritz (1995), Scaling and uncertainty in the relationship between NDVI and land surface biophysical variables: An analysis using a scene simulation model and data from FIFE, *Remote Sens. Environ.*, *54*, 233–246.

Hall, F. G., K. F. Huemmrich, S. J. Goetz, P. J. Sellers, and J. E. Nickerson (1992), Satellite remote sensing of surface energy balance: Success, failures and unresolved issues in FIFE, *J. Geophys. Res.*, *97*, 19,061–19,089.

Kustas, W. P., J. M. Norman, M. C. Anderson, and A. N. French (2003), Estimating subpixel surface temperatures and energy fluxes from the vegetation index-radiometric temperature relationship, *Remote Sens. Environ.*, *85*, 429–440.

Li, F., T. J. Jackson, W. P. Kustas, T. J. Schmugge, A. N. French, M. Cosh, and R. Bindlish (2004), Deriving land surface temperature from Landsat 5 and 7 during SMEX02/SMACEX, *Remote Sens. Environ.*, *92*, 521–534.

Norman, J. M., and F. Becker (1995), Terminology in thermal infrared remote sensing of natural surfaces, *Agric. For. Meteorol.*, *77*, 153–166.

Norman, J. M., M. C. Anderson, W. P. Kustas, A. N. French, J. Mecikalski, R. Torn, G. R. Diak, T. J. Schmugge, and B. C. W. Tanner (2003), Remote sensing of surface energy fluxes at 10^1-m pixel resolutions, *Water Resour. Res.*, *39*(8), 1221, doi:10.1029/2002WR001775.

Sobrino, J. A., N. Raissouni, and Z.-L. Li (2001), A comparative study of land surface emissivity retrieval from NOAA data, *Remote Sens. Environ.*, *75*, 256–266.

Willmott, C. J., and K. Matsuura (2005), Advantages of the mean absolute error (MAE) over the root mean square error (RMSE) in assessing average model performance, *Clim. Res.*, *30*, 79–82.

N. Agam, M. C. Anderson, W. P. Kustas, and F. Li, Hydrology and Remote Sensing Laboratory, Agricultural Research Service, U.S. Department of Agriculture, Building 007, BARC-West, Beltsville, MD 20705, USA. (nurit.agam@gmail.com)

P. D. Colaizzi, Conservation and Production Research Laboratory, Agricultural Research Service, U.S. Department of Agriculture, Bushland, TX 79012, USA.